Robertson, A.H.F., Emeis, K.-C., Richter, C., and Camerlenghi, A. (Eds.), 1998
Proceedings of the Ocean Drilling Program, Scientific Results, Vol. 160

41. PRESENT-DAY STRESS INDICATORS FROM A SEGMENT OF THE AFRICAN-EURASIAN PLATE BOUNDARY IN THE EASTERN MEDITERRANEAN SEA: RESULTS OF FORMATION MICROSCANNER DATA[1]

María José Jurado-Rodríguez[2] and Martin Brudy[3]

ABSTRACT

Ocean Drilling Program Leg 160 investigated two segments of the active African-Eurasian plate boundary in the Eastern Mediterranean Sea by shallow drilling: the Eratosthenes Seamount and the Mediterranean Ridge Olimpi mud volcano field. The borehole logging data acquired during Leg 160 were analyzed to obtain stress indicators and a better definition of the present-day stress situation in the Eastern Mediterranean. Both borehole breakout zones (borehole enlargements) and vertical drilling-induced fractures were identified from borehole geometry data recorded using the Formation MicroScanner (FMS) tool and from computer-generated FMS images, respectively. For Holes 966F and 967E at the Eratosthenes Seamount, the enlargements and the drilling-induced fractures show the same orientation. If both were stress induced and representative of the present-day stress orientation, they would be 90° off. A comparison of the strike of the inferred borehole enlargements with the observed paleostress-related fracturing suggests the possibility that borehole enlargements might be aligned with the strike of some of the structures. Thus, we derive the stress orientation at the Eratosthenes Seamount sites from drilling-induced fractures alone. The orientation of the maximum horizontal principal stress, S_H, is about N50°E for Hole 966F, located on the seamount plateau, and N30°E for Hole 967E, located on the northern slope of the Eratosthenes Seamount. For Hole 965A, also on the slope but at a shallower depth, the orientation obtained is about N170°E. The stress orientations obtained from borehole enlargements and from the vertical drilling-induced fractures in Hole 970A, on the eastern flank of the Milano mud volcano, show consistent, nearly north–south, orientations of S_H.

INTRODUCTION

The tectonic framework of the Eastern Mediterranean shown in Figure 1 is dominated by the collision of the Arabian and African Plates with Eurasia (McKenzie, 1970). Drilling during Ocean Drilling Program (ODP) Leg 160 had two major scientific objectives: to investigate (1) the role of the Eratosthenes Seamount in the tectonic evolution of the Eastern Mediterranean (Robertson and Shipboard Scientific Party, 1996), and (2) the mud volcanism in the Mediterranean Ridge, related to an incipient collisional setting (Cita and Camerlenghi, 1992; Cita et al., 1996; Camerlenghi et al., 1992, 1995; Fig. 1).

The Eratosthenes Seamount (Fig. 1) is a unit of inferred African continental origin. South of Cyprus, analysis of earthquake focal mechanisms suggests that basement faults near the continental/ocean boundary of the North African Plate were reactivated as compressional structures in possible response to collision of the Eratosthenes Seamount with the North African continental margin (Ben Avraham and Nur, 1986). In the easternmost Mediterranean, earthquake data suggest that northeastward subduction locally persists beneath southwest Cyprus (Kempler and Ben Avraham, 1987). Recent evidence of seismicity indicates that seismic activity along the Cyprus arc occurs in a wide seismogenic belt, which has been related to the borders of Sinai subplate (Salamon et al., 1996). Major and moderate earthquakes are concentrated in southwestern and southeastern Cyprus, and also toward the Eratosthenes Seamount to the south. These events are associated with compressional structures that are interpreted in relation to northward subduction (Salamon et al., 1996). Strong uplift of Cyprus, including the Troodos Massif and the Kyrenia Range, has been attributed to the effects of collision and underthrusting of the Eratosthenes Seamount (Robertson et al., 1991). Uplift in Cyprus was most intense during the late Pliocene–middle Quaternary, possibly reflecting underthrusting of buoyant crust (Robertson and Grasso, 1995). This was followed by reduced rates of uplift after the middle Pleistocene (Poole and Robertson, 1991). On a regional scale, the stress situation can be expected to be rather complex if the existence of neighboring transform fault zones to the north (Anatolian: Robertson and Grasso, 1995; Troodos: MacLeod and Murton, 1995) is considered.

Three holes were drilled and geophysically logged at the Eratosthenes Seamount during Leg 160: Hole 966F (356 m deep) on the seamount plateau, and Holes 965A (250.4 m deep) and 967E (600.3 m deep) on its northern slope (Fig.1).

Results from Leg 160 (Robertson and Shipboard Scientific Party, 1996) indicate that deep-water pelagic sediments of late Mesozoic age were deposited in a stable tectonic setting adjacent to the passive continental margin of North Africa. Shallow-water carbonate was deposited on the Eratosthenes Seamount during the Miocene. This was associated with tectonic uplift, followed by rapid subsidence (interpreted as the consequence of extensional faulting and breakup) to water depths of up to 2000 m after early Pliocene time.

The Mediterranean Ridge is now recognized as a mud-dominated accretionary wedge (Kastens, 1991) that has evolved as an accretionary prism built up by offscraping of sediments deposited on the downgoing plate (Lallemant et al., 1994). These authors outline a transition from compression in the Western Mediterranean to extension in the Aegean area. In a stress distribution sketch of the Mediterranean Ridge, Lallemant et al. (1994) interpret the least principal stress, S_3, to be vertical in the outer and central units of the Mediterranean Ridge accretionary complex and the maximum principal stress, S_1, to be perpendicular to the ridge. From microseismicity data, Hatzfeld et al. (1993) deduced that the azimuth of the Crete/Africa relative motion is about N25°.

[1]Robertson, A.H.F., Emeis, K.-C., Richter, C., and Camerlenghi, A. (Eds.), 1998. *Proc. ODP, Sci. Results*, 160: College Station, TX (Ocean Drilling Program).

[2]Geophysikalisches Institut, Universität Fridericiana Karlsruhe, Hertzstrasse 16, 76187 Karlsruhe, Federal Republic of Germany. Present address: Instituto de Ciencias de la Tierra, Lluis Solé Sabarís s/n, 08028 Barcelona, Spain. mjjurado@ija.csic.es

[3]Geophysikalisches Institut, Universität Fridericiana Karlsruhe, Hertzstrasse 16, 76187 Karlsruhe, Federal Republic of Germany. Present address: Statoil, Trondheim, Norway.

Prior Chapter Contents Next Chapter

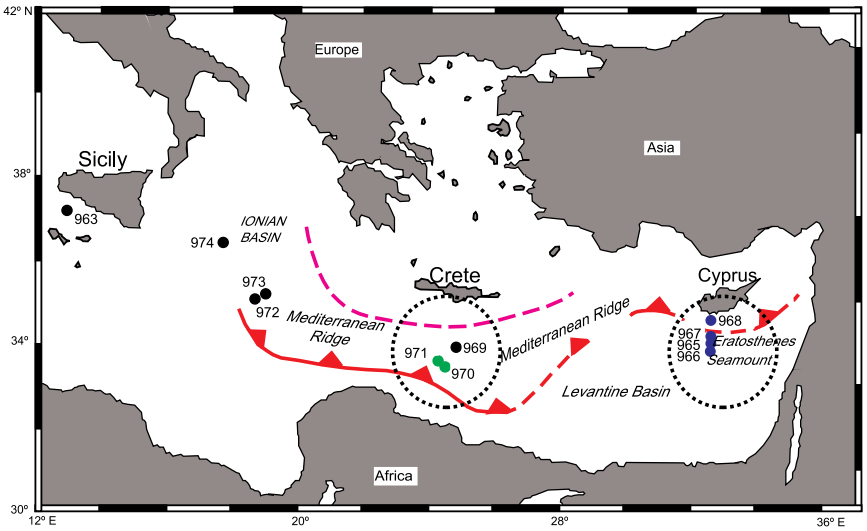

Figure 1. Location map of Leg 160 sites. The dashed circles indicate the sites analyzed in this study.

The material extruded at the mud volcanoes of the Mediterranean Ridge is mainly mud breccia (Cita et al., 1981), with centimeter-sized lithic clasts.

Holes in the Milano and Napoli mud volcanoes were drilled at ~2000 m water depth on the crest areas and across the flanks of the mud volcanoes (Emeis, Robertson, Richter, et al., 1996; Robertson and Shipboard Scientific Party, 1996). At Site 970, pelagic, layered, host sediments were also recovered (Emeis, Robertson, Richter, et al., 1996), interbedded with mud breccia. Hole 970A (201.4 m), on the flank of the Milano mud volcano, and Hole 971B (203.5 m), on the flank of the Napoli mud volcano, were geophysically logged. Logging data constitute the most complete record of the sediments drilled at the Napoli and Milano mud volcanoes, given the partial core recovery.

The purpose of this study is to analyze newly acquired Leg 160 borehole data to obtain stress indicators for a segment of the African-Eurasian plate boundary in the Eastern Mediterranean and to interpret these results in the context of their geodynamic setting and relationship with other present-day stress indicators. The results obtained raise questions about the degree to which the data are representative of crustal stresses and about the causes of discrepancies found between borehole enlargements and vertical drilling-induced fractures in two of the holes.

METHODS AND DATA

The data analyzed, borehole geometry logs, and Formation MicroScanner (FMS) images were acquired in two successive passes using a slimhole FMS tool. A slimhole tool is required because the logging tools pass through the drill pipe into the borehole, so the tool diameter must be smaller than the pipe diameter. Logging using a slimhole tool results in low coverage of the borehole wall. FMS data were processed and analyzed following standard procedures (Ekstrom et al., 1987; Harker et al., 1990; Bourke, 1989).

Stress indicators were detected in Holes 965A, 966F, 967E, and 970A, which are all relatively shallow (200–600 mbsf). Holes 965A and 967E are situated on the northern slope of the Eratosthenes Seamount, and Hole 966F is on its plateau. Hole 970A is located on the flank of the Milano mud volcano. Water depths for these holes range from 2000 to 3000 m (Hole 965A: 1517.7 m; Hole 966F: 934 m; Hole 967E: 2564 m; and Hole 970A: 2086.2; Emeis, Robertson, Richter, et al., 1996). The data obtained in Hole 968A and 971B were of insufficient quality to allow analysis of stress indicators.

Two different types of stress indicators were analyzed in this study to infer the orientation of the horizontal principal stresses: borehole breakouts and vertical drilling-induced fractures. Breakouts are diametrically opposed zones of compressional failure of the borehole wall in a direction perpendicular to the orientation of the maximum horizontal principal stress, S_H. They occur as a consequence of stress concentration around a borehole drilled into anisotropically stressed rock (Bell and Gough, 1979, 1983; Gough and Bell, 1981; Cox, 1983; Zoback et al., 1985; Plumb and Hickman, 1985). In numerous studies, borehole breakouts have proven to be reliable indicators of the orientation of the horizontal principal stresses (e.g., Hickman et al., 1985; Zoback et al., 1989; Moos and Zoback, 1990; Shamir and Zoback, 1992). In this study, the breakout analysis was performed on logs of oriented four-arm calipers recorded using the slimhole FMS tool. The individual borehole breakouts are identified following the criteria of Plumb and Hickman (1985), except that the smaller caliper was usually larger than the bit. ODP drilling and coring systems tend to form holes of relatively large diameter, as was the case for the holes analyzed in this study. Therefore, most of the enlargements we identified in this study do not strictly fulfill the breakout criteria of Plumb and Hickman (1985) and are thus referred to below as oriented borehole enlargements, rather than as breakouts. Nevertheless, we believe the intervals identified as oriented borehole enlargements reflect preferentially oriented zones of failure of the borehole wall caused by stress concentration around the borehole (Kirsch, 1898).

Vertical drilling-induced fractures are tensile failures of the borehole wall that form in the direction of the maximum horizontal principal stress, S_H, at the borehole wall (Brudy et al., 1997). Because these fractures are filled with drilling mud, their electrical conductivity differs from that of the host rock, which allows them to be detected in high-resolution images of the electrical conductivity of the borehole wall (FMS measurements). An example from Hole 966A is given in Figure 2. The vertical drilling-induced fractures are seen as traces of high conductivity subparallel to the borehole axis, 180° apart at the borehole wall. They can easily be distinguished from natural, nonvertical fractures, which appear as sinusoidal traces on FMS images. Their initiation may relate to increased drilling-fluid pressure during drilling operation and to cooling of the rock by circulation of relatively cold drilling mud (Brudy et al., 1997). Vertical drilling-induced fractures were identified in FMS images for Holes 965A, 966F, 967E, and 970A. The interpretation of borehole breakouts and drilling-induced fractures as stress indicators is made under the assumption that one principal stress parallels the borehole axis. Because all analyzed boreholes are nearly vertical, this amounts to an

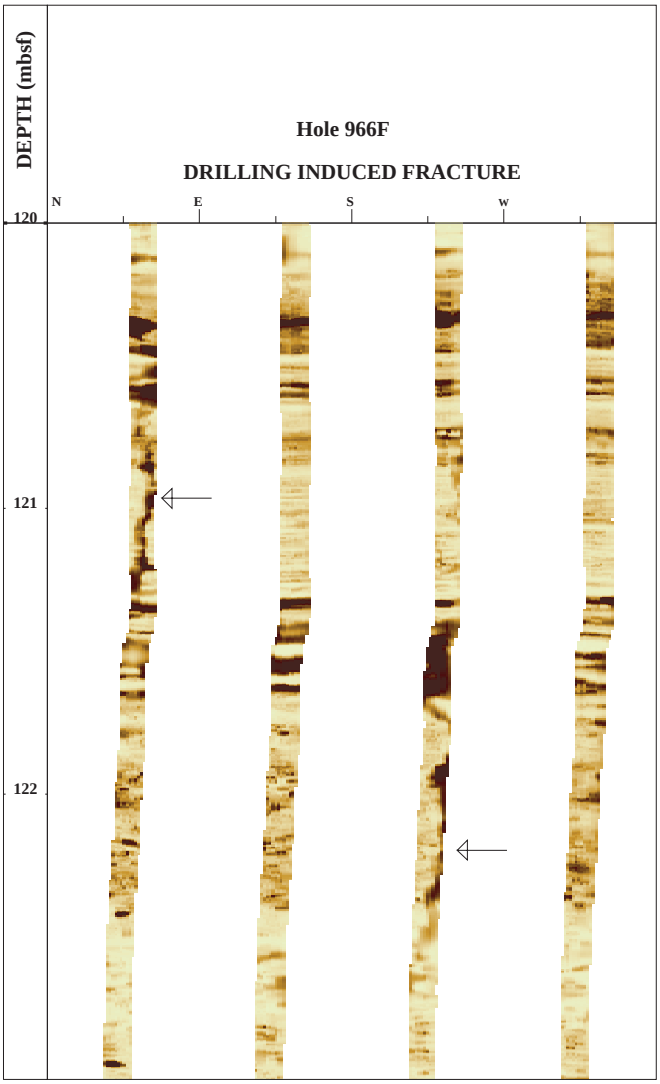

Figure 2. Drilling-induced vertical fractures are visible in FMS images as narrow bands of increased conductivity, 180º from the borehole wall. They are subparallel to the borehole axis and crosscut the bedding planes, seen as sinusoidal structures. The figure shows a Hole 966F FMS image where the two fractures have a slight depth offset (one fracture has an orientation of about N50ºE at about 121 m depth, and the other has an orientation of about N230ºE at 122 m depth).

assumption that the vertical stress, which is calculated as the overburden load, is a principal stress.

STRESS ORIENTATION RESULTS

The orientations of breakouts and drilling-induced fractures in Holes 965A, 966F, 967E, and 970A are shown in Figures 3–6. The intervals identified as borehole enlargements are indicated by lines of different thickness (the thicker the line, the better the quality of the value). The orientations obtained for drilling-induced fractures are indicated by squares (crosses in Fig. 6).

The oriented calipers of the four-arm FMS tool reveal the existence of several segments of borehole enlargements in each hole, ranging in length from 5 to 40 m. In Holes 966F and 967E, most of the vertical drilling-induced fractures form in the direction of the borehole enlargements. A typical case is seen at a depth of about 190–240 m in Hole 967E (Fig. 5). In Hole 970A, the borehole breakouts and vertical drilling-induced fractures occur 90° off, as expected for unfractured, isotropic rock.

In intact rock, breakouts form by compressive failure of the rock in two zones of maximum tangential stress around the borehole in the direction perpendicular to the orientation of S_H. In a fractured rock mass, if the fractures strike parallel to S_H, then, close to the borehole wall, only the minimum tangential stress around the hole acts in a direction normal to the fracture planes. Therefore, if a borehole is drilled in such an environment, fractures may tend to open, especially where mud pressure is increased during drilling (Haimson et al., 1984). This mechanism could result in enlargements of the borehole cross section in the direction of S_H, which could not be differentiated by four-arm caliper analysis from breakouts caused by compressional failure.

PRELIMINARY FRACTURE INTERPRETATION RESULTS

To test if fracturing could have influenced the formation of breakouts in the boreholes at the Eratosthenes Seamount, we compared the breakout orientation to the paleostress and preliminary fracture interpretation data from Holes 965A, 966F, and 967E. In Hole 965A (Fig. 3), the breakout orientation does obviously correlate with fractures, although the two shallowest breakouts parallel the strike of some fractures. In Hole 966F (Fig. 4), both borehole breakouts and vertical fractures parallel the strike of some paleostress-related fractures. Because of the scarcity of fracture data, the fractures do not show any clear azimuthal distribution, and we cannot determine whether the breakouts are aligned with any of the fracture sets interpreted from FMS images. The same applies to Hole 967E (Fig. 5).

In Hole 970A, the stress orientations derived from breakouts and drilling-induced fractures are rather consistent, with a mean orientation of N170°E to N180°E (Fig. 6). Unfortunately, only one pair of drilling-induced fractures at about 182 m depth could be identified in the FMS images.

DISCUSSION

Both the Eratosthenes Seamount and the Mediterranean Ridge mud volcano field are located in a compressive tectonic regime. Our analysis of Leg 160 borehole data does not allow to derive with certainty a present-day stress orientation for Eratosthenes, but the results are more conclusive for Site 970 on the Mediterranean Ridge.

The stress indicators included in the World Stress Map database (Zoback, 1992) do not show any clearly defined stress pattern for the Eratosthenes Seamount or the Milano mud volcano areas. However, our data can be compared to stress information obtained from neighboring areas. The nearest information to the Eratosthenes Seamount comes from a study of stress and fracturing undertaken by Haimson et al. (1984) on Cyprus. Hydraulic fracturing stress measurements and analysis of borehole televiewer logging data for breakout occurrence show an orientation of N70°E ± 10° for S_H in the shallowest 600 m of the CY-4 drillhole. In that study, breakouts were interpreted to occur in zones of intense fracturing in the direction N65°E ± 25°, which is subparallel to the strike of a northeastern, steeply inclined fracture set, which thus suggests a similar direction for S_H. Breakouts would then be aligned normal to the minimum horizontal in situ stress. Hydraulic fracturing results indicate potential normal or/and strike-slip faulting. Haimson et al. (1984) suggest that the east–west

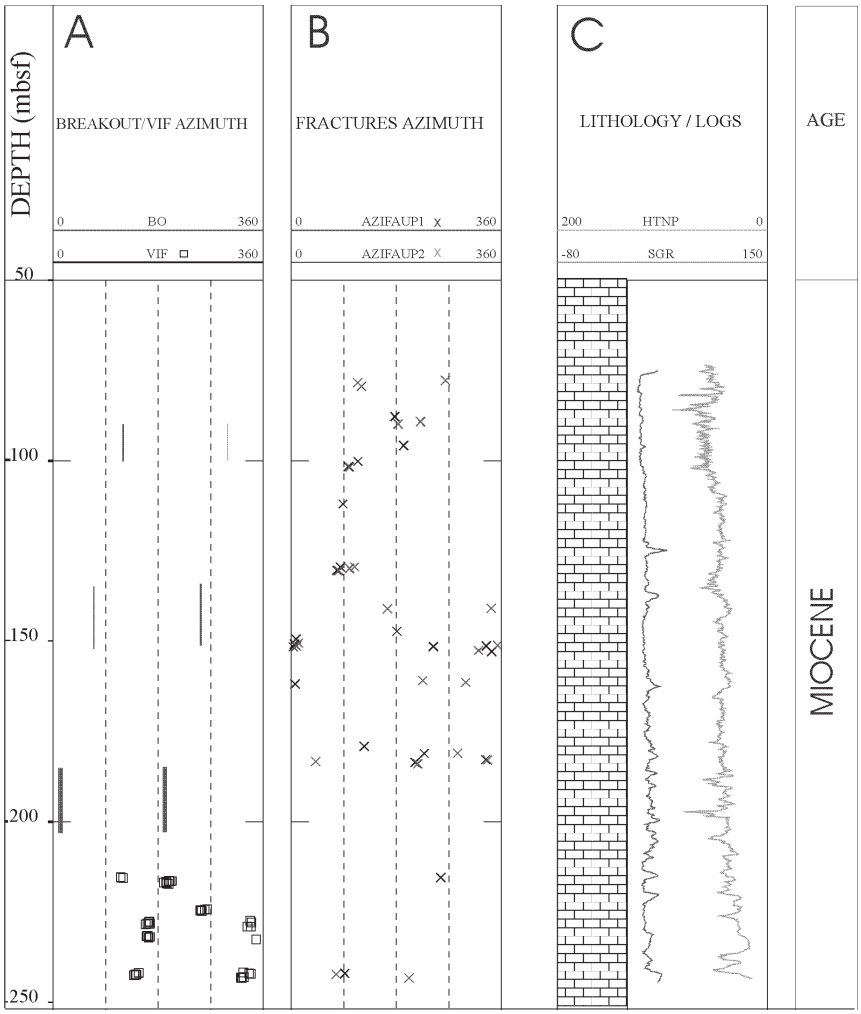

Figure 3. Hole 965A. **A.** Orientation of borehole enlargements (BO, continuous line) and vertical drilling-induced fractures (VIF, squares). **B.** Paleostress-related fracturing measured on pass-1 FMS images (AZIFAUPI1) and pass-2 images (AZIFAUPI2); strike of the fractures. **C.** Lithologic column (carbonates), spectral natural gamma-ray log (SGR, API units), and neutron log (HNTP, apparent porosity units).

plate boundary near Cyprus could be undergoing left-lateral strike-slip faulting.

The situation at the Eratosthenes Seamount might be similar. The fact that borehole enlargements and vertical drilling-induced fractures that we identified at Holes 966F and 967E are aligned may result from preferential orientation of borehole enlargements in a direction of weakness coincident with fault strikes. A more complete data set is required to confirm this hypothesis. If correct, the drilling-induced fractures could represent the orientation of S_H, with a north–northeast to south–southwest orientation of S_H for Holes 966F and 967E (N30°E and N50°E, respectively). In Hole 965A, the drilling-induced fractures, and thus also S_H, are oriented approximately N170°E, although orientations are scattered.

Another possible interpretation for the situation at Eratosthenes is that the "drilling-induced fractures" actually represent an incipient stage of development of borehole breakouts and thus are aligned with the borehole enlargements observed in Holes 966F and 967E. Such a possibility was suggested by A. Krammer (pers. comm., 1997). In this case, S_H would be located 90° away from the orientation obtained for these holes.

Hole 970A shows the most consistently oriented borehole enlargements of the boreholes investigated. This is remarkable, as this hole was drilled into a mud volcano and penetrated sediments that do not deform strictly elastically and have very low compressive rock strength. The results obtained for the Milano mud volcano are consistent with the stress distribution proposed by Lallemant et al. (1994) for the outer and central units of the Mediterranean Ridge accretionary prism for S_H, which is perpendicular to the ridge strike. Nevertheless, Hieke et al. (1996), in a geomorphologic study of the Milano and the Napoli mud volcanoes, note the existence of lineations that they interpret as a system of fractures on the seafloor. The resulting north–south orientation of S_H is subparallel to the collision front.

CONCLUSIONS

1. The results obtained are difficult to interpret in the case of the Eratosthenes Seamount (Holes 965A, 966F, and 967E), but are consistent for the Milano mud volcano (Hole 970A).
2. Borehole enlargements and vertical drilling-induced fractures tend to have the same orientation on the Eratosthenes Seamount. Consequently, a discrepancy exists between the orientation derived for S_H from borehole enlargements and that obtained from vertical drilling-induced fractures. Alignment of borehole enlargements and vertical drilling-induced fractures could be explained if the borehole enlargements formed in the direction of S_H, related to fractures striking parallel to the S_H orientation.

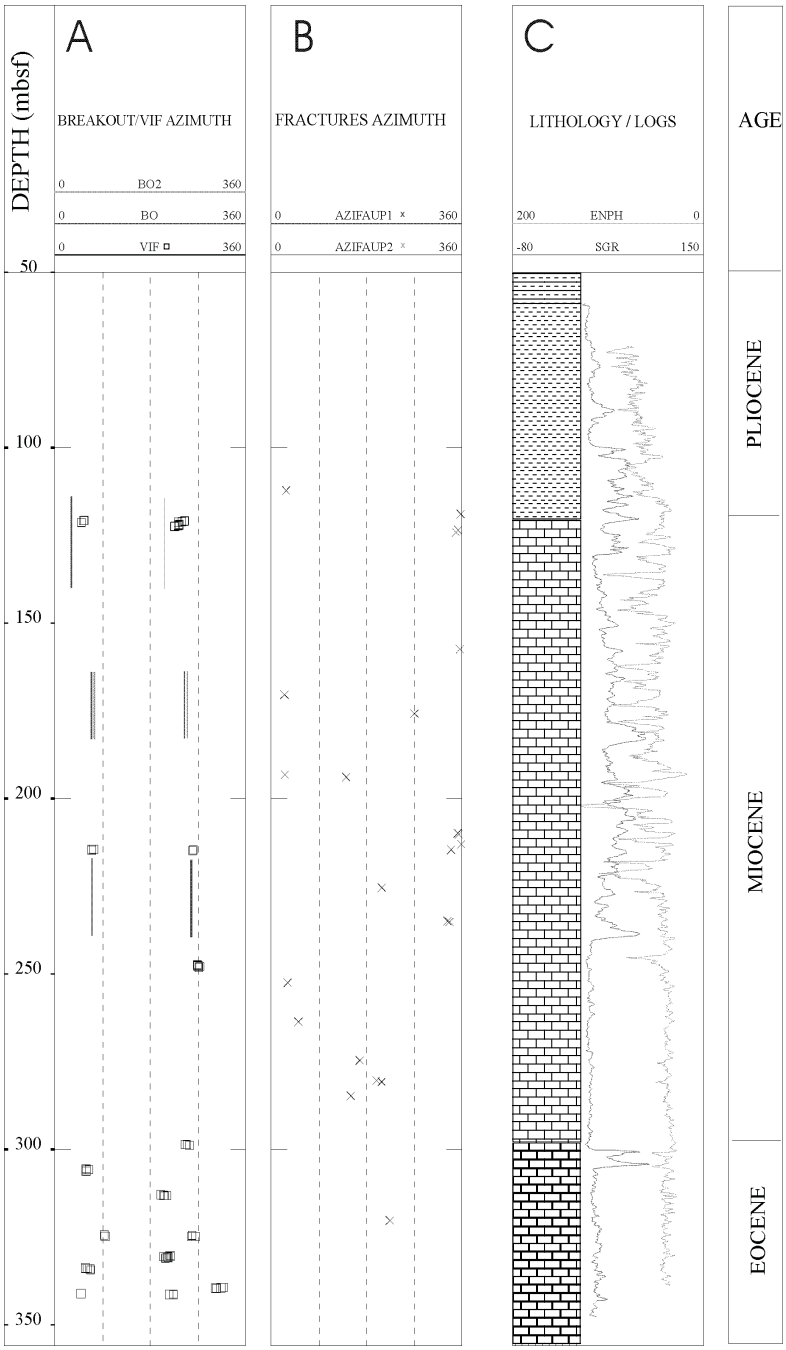

Figure 4. Hole 966F. **A.** Orientation of borehole enlargements (BO, continuous line) and vertical drilling-induced fractures (VIF, squares). **B.** Paleostress-related fracturing measured on pass-1 FMS images (AZIFAUPI1) and pass-2 images (AZIFAUPI2); strike of the fractures. **C.** Lithologic column, spectral natural gamma-ray log (SGR, API units), and neutron log (ENPH, apparent porosity units). Lithologic patterns from top to bottom = clay, breccia, and carbonates.

3. S_H indicators strike approximately north–south in the Milano mud volcano. This result is consistent with compression perpendicular to the edge of the Mediterranean Ridge.
4. For the Eratosthenes Seamount, a north–northeast to south–southwest orientation is tentatively proposed from analyses of Holes 966F and 967E, although data from Hole 965A tend to indicate a stress orientation of approximately N170°E.
5. A correlation between the deduced maximum horizontal stress orientations and the strike of some of the same, nearly north-south–striking, shallow fractures may be made for Hole 965A.

ACKNOWLEDGMENTS

We thank Alastair Robertson and anonymous reviewers for helpful criticism and suggestions.

REFERENCES

Bell, J.S., and Gough, D.I., 1979. Northeast-southwest compressive stress in Alberta: evidence from oil wells. *Earth Planet. Sci. Lett.*, 45:475–482.

————, 1983. The use of borehole breakouts in the study of crustal stress. *In* Zoback, M.D., and Haimson, B.C. (Eds.), *Hydraulic Fracturing Stress Measurements:* Washington (National Academy Press), 201–209.

Ben-Avraham, Z., and Nur, A., 1986. Collisional processes in the Eastern Mediterranean. *Geol. Rundsch.,* 75:209–217.

Bourke, L.T., 1989. Recognizing artifact images of the formation microscanner. *SPWLA 30th Ann. Logging Symp.*, paper WW.

Brudy, M., Zoback, M.D., Fuchs, K., Rummel, F., and Baumgärtner, J., 1997. Estimation of the complete stress tensor to 8 km depth in the KTB scientific drill holes—implications for crustal strength. *J. Geophys. Res.* 18453–18475.

Camerlenghi, A., Cita, M.B., Della Vedova, B., Fusi, N., Mirabile, L., and Pellis, G., 1995. Geophysical evidence of mud diapirism on the Mediterranean Ridge accretionary complex. *Mar. Geophys. Res.,* 17:115–141.

Camerlenghi, A., Cita, M.B., Hieke, W., and Ricchiuto, T.S., 1992. Geological evidence for mud diapirism on the Mediterranean Ridge accretionary complex. *Earth Planet. Sci. Lett.,* 109:493–504.

Cita, M.B., and Camerlenghi, A., 1992. The Mediterranean Ridge as an accretionary prism in collision context. *Mem. Soc. Geol. Ital.,* 45:463–480.

Cita, M.B., Ivanov, M.K., and Woodside, J., 1996. The Mediterranean Ridge diapiric belt: introduction. *Mar. Geol.,* 132:1–6.

Cita, M.B., Ryan, W.B.F., and Paggi, L., 1981. Prometheus mud-breccia: an example of shale diapirism in the Western Mediterranean Ridge. *Ann. Geol. Pays Hellen.,* 30:543–570.

Cox, J.W., 1983. Long axis orientation in elongated boreholes and correlation with rock stress data. *24th Ann. Log. Symp.,* 1983:1–17.

Ekstrom, M.P., Dahan, C., Chen, M.-Y., Lloyd, P., and Rossi, D.J., 1987. Formation imaging with microelectrical scanning arrays. *Log Analyst,* 28:294–306.

Emeis, K.-C., Robertson, A.H.F., Richter, C., et al., 1996. *Proc. ODP, Init. Repts.,* 160: College Station, TX (Ocean Drilling Program).

Gough, D.I., and Bell, J.S., 1982. Stress orientations from borehole wall fractures with examples from Colorado, East Texas, and northern Canada. *Can. J. Earth Sci.,* 19:1358–1370. [Ed: was listed as 1981]

Haimson, B.C., Lee, M.Y., Baumgärtner, J., and Rummel, F., 1984. Plate tectonics and structure inferences from in situ stress measurements and fracture logging in drillhole CY-4, Troodos ophiolite, Cyprus. *In* Malpas, J., Moores, E.M., Paryiotra, A., and Xenophontos, C. (Eds.), *Ophiolites: Oceanic Crustal Analogues.* Proc. Symp. "Troodos 1987." Nicosia, Cyprus. Geol. Surv. Dept, Nicosia, 131–138.

Harker, S.D., McGann, G.J., Bourke, L.T., and Adams, J.T., 1990. Methodology of Formation Micro Scanner image interpretation in Claymore and Scapa Fields (North Sea). *In* Hurst, A., Lovell, M.A., and Morton, A.C. (Eds.), *Geological Applications of Wireline Logs.* Geol. Soc. Spec. Publ. London, 48:11–25.

Hatzfeld, D., Besnard, M., Makropoulos, K., and Hatzidimitriou, P., 1993. Microearthquake seismicity and fault plane solutions in the southern Aegean and its geodynamics implications. *Geophys. J. Int.,* 115:799–818.

Hickman, S.H., Healy, J.H., and Zoback, M.D., 1985. In situ stress, natural fracture distribution, and borehole elongation in the Auburn Geothermal Well, Auburn, New York. *J. Geophys. Res.,* 90:5497–5512.

Hieke, W., Werner, F., and Schenke, H.W., 1996. Geomorphological study of an area with mud diapirs south of Crete (Mediterranean Ridge). *Mar. Geol.,* 132:63–93.

Kastens, K., 1991. Rate of outward growth of the Mediterranean Ridge accretionary complex. *Tectonophysics,* 199:25–50.

Kempler, D., and Ben-Avraham, Z., 1987. The tectonic evolution of the Cyprean Arc. *Ann. Tecton.,* 1:58–71.

Kirsch, G., 1898. Die Theorie der Elastizität und die Bedürfnisse der Festigkeitslehre. *VDI Z.,* 42:797–807.

Lallemant, S., Truffert, C., Jolivet, L., Henry, P., Chamot-Rooke, N., and de Voogd, B., 1994. Spatial transition from compression to extension in the Western Mediterranean Ridge accretionary complex. *Tectonophysics,* 234:33–52.

MacLeod, C.J., and Murton, B.J., 1995. On the sense of slip of the Southern Troodos transform fault zone. Cyprus. *Geology,* 23:257–260.

McKenzie, D.P., 1970. Plate tectonics of the Mediterranean region. *Nature,* 226:239.

Moos, D., and Zoback, M.D., 1990. Utilization of observations of well bore failure to constrain the orientation and magnitude of crustal stresses: application to continental, Deep Sea Drilling Project, and Ocean Drilling Program boreholes. *J. Geophys. Res.,* 95:9305–9325.

Plumb, R.A., and Hickman, S.H., 1985. Stress-induced borehole elongation: a comparison between the four-arm dipmeter and the borehole televiewer in the Auburn geothermal well. *J. Geophys. Res.,* 90:5513–5521.

Poole, A.J., and Robertson, A.H.F., 1991. Quaternary uplift and sea-level change at an active plate boundary, Cyprus. *J. Geol. Soc. London,* 148:909–921.

Robertson, A.H.F., Clift, P.D., Degnan, P., and Jones, G., 1991. Palaeogeographic and palaeotectonic evolution of the Eastern Mediterranean Neotethys. *Palaeogeogr., Palaeoclimatol., Palaeoecol.,* 87:289–344.

Robertson, A.H.F., and Grasso, M., 1995. Overview of the Late Tertiary-Recent tectonic and palaeo-environmental development of the Mediterranean region. *Terra Nova,* 7:114–127.

Robertson, A.H.F., and Shipboard Scientific Party, 1996. Role of the Eratosthenes Seamount in collisional processes in the Eastern Mediterranean. *In* Emeis, K.-C., Robertson, A.H.F., Richter, C., et al., *Proc. ODP, Init. Repts.,* 160: College Station, TX (Ocean Drilling Program), 513–520.

Salamon, A., Hofstetter, A., Garfunkel, Z., and Ron, H. 1996. Seismicity of the eastern Mediterranean region: perspective from the Sinai subplate. *Tectonophysics,* 263:293–305.

Shamir, G., and Zoback, M.D., 1992. Stress orientation profile to 3.5 km depth near the San Andreas Fault at Cajon Pass, California. *J. Geophys. Res.,* 97:5059–5080.

Zoback, M.D., Moos, D., Mastin, L., and Anderson, R.N., 1985. Well bore breakouts and in situ stress. *J. Geophys. Res.,* 90:5523–5530.

Zoback, M.L., 1992. First- and second-order patterns of stress in the lithosphere: the world stress map project. *J. Geophys. Res.,* 97:11703–11728.

Zoback, M.L., Zoback, M.D., Adams, J., Assumpção, M., Bell, S., Bergman, E.A., Blümling, P., Brereton, N.R., Denham, D., Ding, J., Fuchs, K., Gay, N., Gregersen, S., Gupta, H.K., Gvishiani, A., Jacob, K., Klein, R., Knoll, P., Magee, M., Mercier, J.L., Müller, B.C., Paquin, C., Rajendran, K., Stephansson, O., Suarez, G., Suter, M., Udias, A., Xu, Z.H., and Zhizhin, M., 1989. Global patterns of tectonic stress. *Nature,* 341:291–298.

Date of initial receipt: 16 January 1997
Date of acceptance: 8 August 1997
Ms 160SR-030

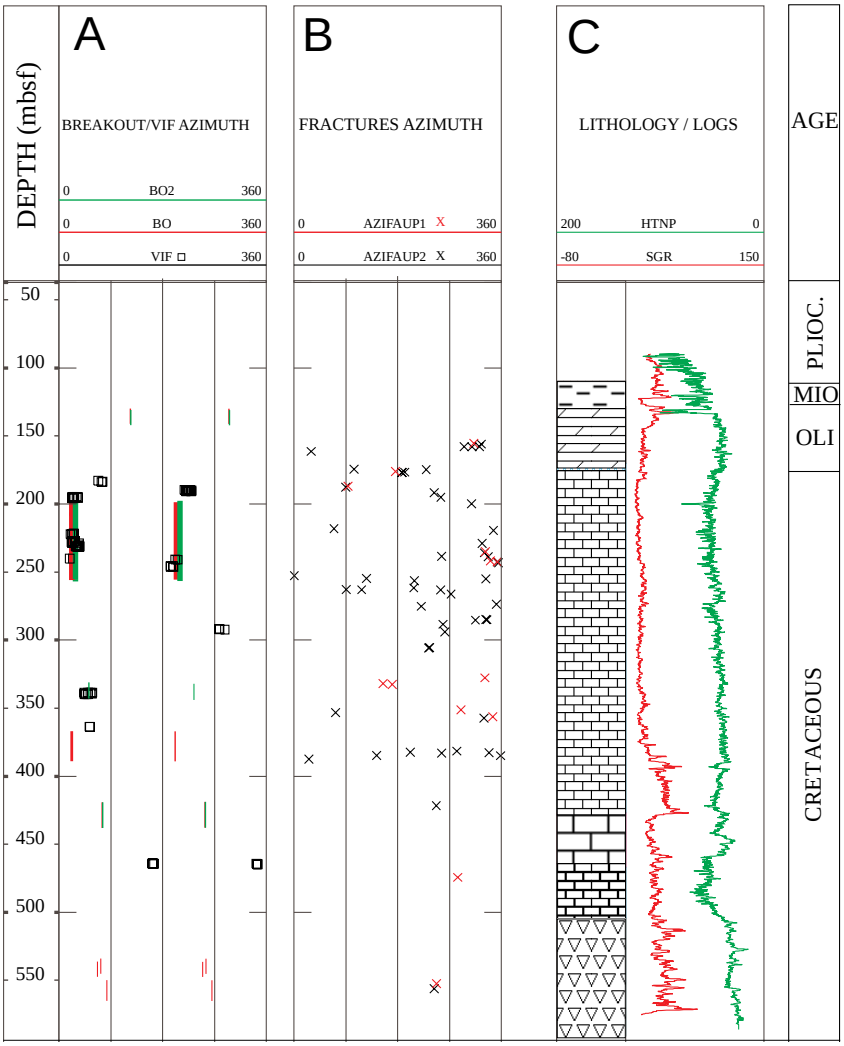

Figure 5. Hole 967E. **A.** Stress indicators obtained from borehole enlargements (BO, continuous line) and vertical drilling-induced fractures (VIF, squares). **B.** Paleostress-related fracturing measured on pass-1 FMS images (AZIFAUPI1) and pass-2 images (AZIFAUPI2). **C.** Lithologic column, spectral natural gamma-ray log (SGR, API units), and neutron log (TNPH, apparent porosity units). Lithologic patterns from top to bottom = clay (first pattern), and to total depth, carbonates (different patterns = different facies).

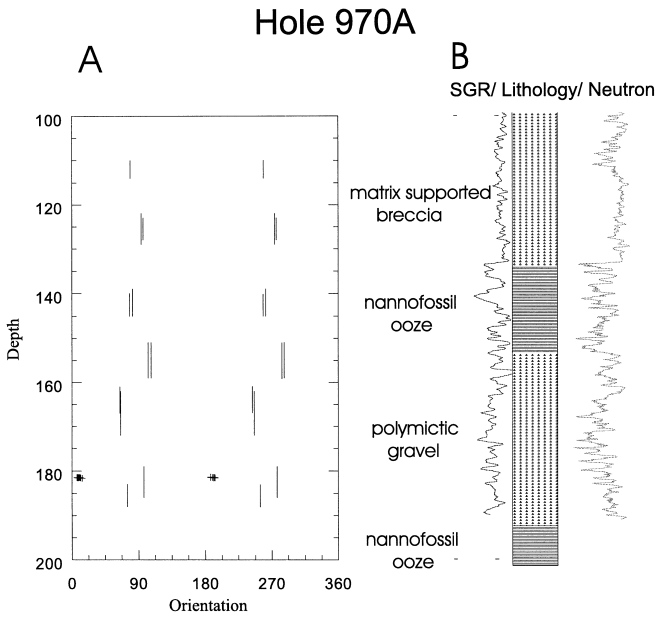

Figure 6. Hole 970A. **A.** Stress indicators obtained from borehole enlargements (continuous line) and vertical drilling-induced fractures (squares). S_H value is represented for both stress indicators. **B.** Lithologic column, spectral natural gamma-ray log (SGR), and neutron logs.

Prior Chapter Contents Next Chapter